Interfacial Electrostatics of Self-Assembled Monolayers of Alkane Thiolates on Au(111): Work Function Modification and Molecular Level Alignments

R. Rousseau,[†] V. De Renzi,*[,‡] R. Mazzarello,[†,§] D. Marchetto,[‡] R. Biagi,[‡] S. Scandolo,[§] and U. del Pennino[‡]

International School for Advanced Studies, 2−4 Via Beirut, 34014 Trieste, Italy, CNR−INFM Center for nanoStructures and bioSystems at Surfaces and Dipartimento di Fisica, Università di Modena e Reggio Emilia, Modena, Italy, and The Abdus Salam International Centre for Theoretical Physics and CNR−INFM/Democritos National Simulation Center, 11 Strada Costiera, 34014 Trieste, Italy

Received: March 20, 2006; In Final Form: March 29, 2006

We have isolated at $T < 150$ K a weakly adsorbed dimethyl disulfide (DMDS) layer on Au(111) and studied how the vibrational states, S core hole level shifts, valence band photoemission, and work function measurements evolve upon transforming this system into chemisorbed methylthiolate (MT) self-assembled monolayers (SAM) by heating above 200 K. By combining these observations with detailed theoretical electronic structure simulations, at the density functional level, we have been able to obtain a detailed picture of the electronic interactions at the interface between Au and adsorbed thiolates and disulfides. All of our measurements may be interpreted with a simple model where MT is bound to the Au surface with negligible charge transfer. Interfacial dipoles arising from Pauli repulsion between molecule and metal surface electrons are present for the weakly adsorbed DMDS layer but not for the chemisorbed species. Instead, for the chemisorbed species, interfacial dipoles are exclusively controlled by the molecular dipole, its interaction with the dipoles on neighboring molecules, and its orientation to the surface. The ramifications of these results for alignment of molecular levels and interfacial properties of this class of materials are discussed.

I. Introduction

In the fields of molecular electronics and organic-based thin film devices, the understanding of the charge-injection process between the metal electrodes and the molecular active species is an issue of paramount importance. Of specific concern is the understanding of how molecule/surface interactions are correlated with the observed modification of properties such as interfacial electrostatics, work function change ($\Delta\Phi$), and alignment between substrate and molecular levels. These properties play a fundamental role in the determination of charge transport across molecule/solid junctions,[1,2] yet their detailed mechanistic understanding is still an open issue.[3−9] In early work, it was generally assumed that the electronic structure of metal−organic interfaces followed the so-called Schottky−Mott limit,[10] according to which the energetic position of molecular levels is given by the alignment of vacuum levels so that the hole- and electron-injection barriers (Φ_h and Φ_e) are obtained by calculating the difference between the work function of the metal (Φ_M) and the ionization energy (IE) and electron affinity (EA) of the organic material, respectively. However, the work done in the past decade revealed a far more complex situation, which can be broadly characterized by a breakdown of the vacuum level alignment rule due to the formation of an interface dipole layer with a corresponding modification of the surface work function.

The interface dipole layer can have different origins: (i) The presence of a molecular intrinsic dipole. In this case, the induced work function variation can have both positive and negative sign, depending on the molecular orientation on the surface. (ii) A charge redistribution or transfer occurring between the metal and the adsorbate upon formation of a chemical bond and/or determined by the energy level alignment.[4,5] (iii) The so-called pillow effect, whereby the electron density spill-out of the clean metal is displaced by Pauli repulsion with the electrons on the adsorbed molecules. This usually corresponds to an effective positive dipole layer.

These factors can be understood in terms of the electronic charge density,[11] but also in a complementary way by employing the electrostatic (Hartree) potential, V_{ES}. This potential is a measure of the electrostatic energy an electron experiences from all the nuclei and other electrons in the system, and thus, for periodic surface slab models where a bulk/surface and vacuum regions can be well defined, provides a direct *quantitative* measure of the system work function and interface dipole layer. As illustrated schematically in Figure 1, with this quantity, the work function is the difference between the Fermi energy of the metal, E_F, and the value of V_{ES} in the vacuum region outside the solid, E_{vac}, and the interfacial dipole layer can be represented as a steplike potential.

The pillow effect is considered to be the cause of the decrease of the metal work function in the case of weakly interacting adsorbates such as alkane molecules[5] and has been recently demonstrated to be the dominant origin of the interface dipole responsible for $\Delta\Phi$ in the case of Xe adsorption on metal surfaces.[12,13] However, the extension of this finding to more complex molecular systems is still an open issue, especially in the case of chemisorbed species.[8,11] Several examples show that

* Corresponding author. E-mail: derenzi.valentina@unimore.it. Telephone: +39 059 2055242. Fax: +39 059 2055235.
[†] International School for Advanced Studies.
[‡] CNR−INFM Center for nanoStructures and bioSystems at Surfaces and Dipartimento di Fisica, Università di Modena e Reggio Emilia.
[§] The Abdus Salam International Centre for Theoretical Physics and CNR−INFM/Democritos National Simulation Center.

10.1021/jp061720g CCC: $33.50
Published on Web 05/13/2006

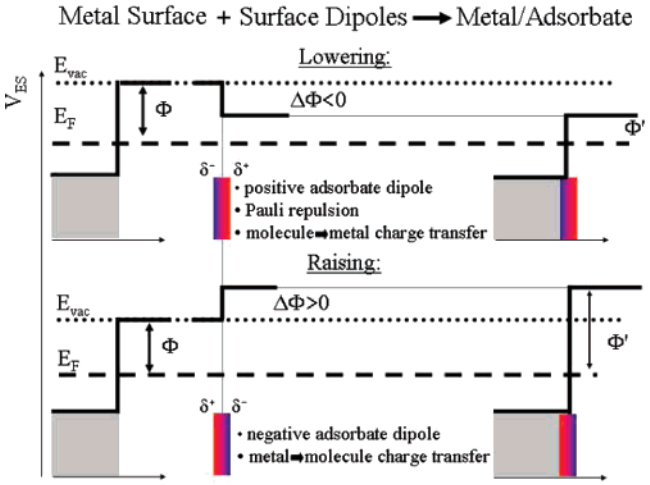

Figure 1. Schematic representation of factors that may influence the observed values of $\Delta\Phi$ at a metal surface. The shape of V_{ES} at the crystal boundary is schematized as a step function for simplicity.

a subtle relationship between charge transfer,[4,14−16] level alignment, and bond formation can occur in strongly interacting interfaces and that significant progress in the comprehension of such interplay could derive from a combined theoretical and experimental study of appropriate model systems.

Among the class of strongly interacting organic−metal interfaces, self-assembled monolayers (SAMs) of sulfur-containing organic molecules on gold are of particular interest[17] due to the central role they play in molecular electronic devices,[18] biosensors,[19] surface coatings, and nanolithography.[20] Even for these well studied materials, there are at least two mutually exclusive pictures of the interfacial electrostatics currently in the literature. On one hand, early theoretical studies suggest that a metal → molecule charge transfer occurs.[21−24] Although more recent density functional theory (DFT) based studies[25−30] indicate that the charge transfer to the thiolate is much smaller than initially thought, this charge-transfer picture is still invoked in order to explain the observed S 2p core hole level shifts for chemisorbed thiolates.[31] This issue is most topical in the context of the recent observation of giant magnetic effects observed for monolayers of alkanethiols adsorbed on Au substrates.[32] Although it is known that even small amounts of charge transfer at a molecule−metal interface[33] can have large nonlocal effects on the materials properties, the currently proposed explanation for this latter phenomena requires "significant amounts" of charge transfer in order to form triplet states confined within domains in the organic layer.[34] However, there is mounting indirect evidence from kelvin probe[35] and photoemission[36] studies of a series of thiolate/Au SAMs that suggests that charge transfer in these materials is indeed small and plays a negligible role in the interfacial electrostatics. To address these issues, we have undertaken a detailed ultraviolet and X-ray photoemission (UPS, XPS) and high-resolution electron energy loss spectroscopy (HREELS) study combined with first principles electronic structure calculations to probe the interfacial electrostatics of adsorbed dimethyl disulfide, $(CH_3S)_2$ (DMDS), and methylthiolate, CH_3S (MT), on the Au(111) surface. DMDS is known to adsorb dissociatively on Au(111) at $T > 200$ K by rupturing the central S−S bond, forming a stable-ordered MT monolayer. In their pioneering work, Nuzzo and co-workers[37] suggested the occurrence of noncomplete DMDS dissociation upon adsorption at low temperature (150 K), as indicated by the shape of the S 2p core level. Moreover, the existence of a metastable DMDS phase has been theoretically predicted by Vargas et al.,[38] for which an adsorption energy of about 0.2 eV was calculated. In a recent letter, we provided first experimental evidence that a metastable phase of weakly adsorbed DMDS exists at $T <$ 150 K.[27] This phase, referred to here as a DMDS layer, evolves into the strongly adsorbed MT by simply increasing the temperature above 200 K. This provides us with a unique route for investigating the evolution of the interface electronic properties upon switching from weak adsorption to chemisorption by simply increasing the temperature. In this work, we characterize these two phases, both from the experimental and theoretical point of view, providing a complete picture of their electronic properties.

II. Experimental and Computational Methods

A. Experimental Methods. All measurements were performed in a UHV chamber with base pressure 7×10^{-11} mbar. The Au sample was cleaned through sputtering−annealing cycles (Ar^+, $E_p = 1$ keV) to 730 K, while DMDS was dosed in the chamber through a leak valve, after pump−freeze−thaw purification cycles. Typical exposure pressures were in the low 10^{-8} mbar. X-ray photoemission measurements were performed by using an unmonochromatized X-ray source and a cylindrical mirror analyzer (CMA). Although the instrumental energy resolution (considered as the fwhm of a typical core-level peak) is rather poor (about 2 eV), the uncertainty in the determination of a single core level peak position, based on a fitting procedure, is about ±0.2 eV. The energy resolution of the UPS valence band spectra was about 200 meV, as determined by the Fermi edge width. Work function changes upon adsorption have been experimentally obtained by measuring the energy position of the secondary edge in the UPS valence band spectra. HREELS measurements were performed with a Leybold ELS 22 spectrometer in specular geometry ($\theta_{in} = \theta_{out} = 60°$), with primary beam energy of 4.2 eV and energy resolution better than 6 meV. At room temperature, DMDS is known to adsorb dissociatively, and a saturation coverage of one monolayer, corresponding to the $(\sqrt{3} \times \sqrt{3})R30°$, was reached for 5 Langmuir (1 Langmuir (L) ≡ 1.33×10^{-6} mbar•s) exposures. At low temperature (100 K), a molecularly adsorbed DMDS first layer is observed, followed by the formation of a physisorbed multilayer. One monolayer (ML) is defined for both DMDS and MT species as the amount of molecules necessary to complete the first layer, with a 1:3 S/Au ratio. Most of the here-reported low-temperature measurements refer to a $T = 100$ K exposure of 3 Langmuir DMDS, which corresponds to a coverage of about 0.6 monolayer as determined by XPS. This choice derives from the need to minimize the possible amount of DMDS molecules physisorbed on top of the first layer so that their contribution to UPS and XPS signals can be safely neglected. We noted that prolonged exposure to the X-ray source induced dissociation of the low-temperature adsorbed DMDS molecules, as indicated by the strong modifications occurring in both XPS and UPS spectra, as well as in the work function value. For this reason, XPS spectra on the low-temperature DMDS phase were obtained by summing up more than 10 short measurements (acquisition time <10 min) on freshly prepared surfaces. On the contrary, even prolonged UV exposure was found not to affect the low-temperature DMDS system.

B. Computational Approach. Electronic structure calculations were performed within the gradient-corrected density functional approximation[39] by employing periodic boundary conditions and norm-conserving pseudopotentials using a plane-wave basis set with energy cutoff of 45 Ry. Specifically, we employed an 11-valence electron potential for Au of the

TABLE 1: Geometric and Electrostatic Properties of Theoretical Structures of DMDS and MT on Au(111) at Full Coverage[a]

	d_{Au-S} Å	z_S Å	Θ_{tilt}	$E_{binding}$ eV	$\Delta\Phi$ eV	ΔE^{init}_{S2p} eV	ΔE^{fin}_{S2p} eV
DMDS-1	2.85	2.7	57	0.2	−1.6	0.0	0.0
DMDS-2	3.35	3.1	56	0.1	−1.6	0.0	−0.4
MT-bridge	2.47	2.0	54	1.1	−1.2	0.1	2.1
MT-ontop	2.36	2.3	64	0.4	−0.6	0.0	2.0
MT-fcc	2.58	2.0	48	0.5	−1.1	0.3	0.6

[a] Tabulated quantities are: the Au−S bond length d_{Au-S}, the height of S above the surface plane z_S, the tilt angle of the S−C bond with respect to the surface normal Θ_{tilt}, the binding energy with respect to 1 mol of DMDS $E_{binding}$, the shift in the work function of the surface relative to that of Au(111), $\Delta\Phi$, The initial state S 2p core hole level shift relative to adsorbed DMDS, ΔE^{init}_{S2p}, and the final state S 2p core hole shift, ΔE^{fin}_{S2p}.

Goedecker type,[40] whereas for S, C, and H, we employed a Troullier−Martins[41] potential. Calculations were carried out with the implementation of the free energy functional for finite electronic temperatures[42] within the CPMD code.[43] Test results indicate that our findings are independent of the electronic temperatures in the range of 0−300 K. As a further cross check and for calculation of projected density of states (DOS), we employed the PWSCF code,[44] with ultrasoft psuedopotentials[45] and Fermi surface smearing. The two methods provide essentially identical structures, DOS and relative energies between configurations, ensuring the reliability of our results beyond the details of the simulation scheme. Validation of our approach by detailed comparison with quantum chemical post-Hartree−Fock correlation methods, including core electrons and localized Gaussian basis sets, has been conducted in our previous work.[26,28]

Binding geometries and energetics of MT and DMDS on Au(111) have been extensively studied by similar methodologies;[22,26,38,46] thus, we focus on the previously reported lowest-energy binding configurations of both species. For MT, we employed a single molecule in a $(\sqrt{3} \times \sqrt{3})$ *R*30° periodic structure, where the MT molecule is located at the bridge, on top, or fcc hollow sites. For DMDS, a c$(3 \times \sqrt{3})$ cell is employed, with initial binding geometries as reported in refs 22, 38, providing an identical 1:3 S/Au ratio as the MT/Au(111) system. All structures were calculated by using a six Au atom thick slab that is periodic in the *x*,*y* plane with an 8−10 Å vacuum layer with fully optimized geometries and converged with respect to Brillouin zone (BZ) integration, with an $8 \times 8 \times 1$ and $4 \times 6 \times 1$ Monkhorst−Pack *k*-mesh[48] for MT and DMDS, respectively. Detailed structural and energetic properties of these "full coverage" MT and DMDS layers are reported in Table 1 and are in excellent accord with previous calculations in the literature.[38,46] Calculations for a S/Au ratio of 1:6 were performed by doubling the unit cells along the shortest cell vector and removing the second adsorbate.

The work function, Φ, is calculated by the difference in energy between E_F and the value of V_{ES} (see ref 49 for the exact definition as implemented within the CPMD code) in the vacuum region between periodic replicas. The dipole layer arising in the vacuum region as a result of the periodic boundary conditions was subtracted, providing a maximum uncertainty of about 0.1 eV in the calculated values of Φ. Calculated $\Delta\Phi$ for full-coverage monolayers of MT and DMDS are provided in Table 1, and see Section 3.B.2 for further discussion. Note that this approach allows us to make direct contact with the experimental measurements and access the interfacial electrostatics yet avoid any form of population analysis and the subsequent arbitrariness this analysis would impose in assigning charges.

Sulfur 2p core hole level shifts are calculated by the effective core hole pseudopotential method of Pasquarello et al.[50] This method allows us to calculate an effective S 2p core hole energy by subtracting the total DFT energy of the ground-state calculation from that of the same system where one of the S atoms is replaced with a pseudo-potential constructed with a hole in the S 2p core state. Initial-state effects may be accessed by calculating the energy of the unrelaxed valence electron density of the ground state with the core hole potential, whereas final-state effects may be evaluated by relaxing the valence electron density to screen the core hole. Because this method provides only reliable chemical shifts, but not absolute core hole ionization energies, we chose as our reference value the lowest-energy configuration of the weakly adsorbed full-coverage DMDS structure. We note that, because this method provides relative shifts with respect to a fixed vacuum level, whereas the experimental measurements are done with respect to a fixed E_F, it is necessary to correct the results by subtracting the change in Φ. Calculated S 2p core hole shifts are provided in Table 1, and see Section 3.B.1 for further discussion.

Reported molecular electronegativities (EN) were obtained from the Mulliken definition, EN = (IP − EA)/2, where IP is the ionization energy. For bulk exposed through its (111) surface, the electronegativity is provided by the fact that the energy to either add or remove an electron relative to the vacuum level E_{vac} is E_F. Hence, for metals, $EN = E_F - E_{vac} = -\Phi$.

III. Results and Discussion

A. Structural and Vibrational Properties. Vibrational properties provide important understanding of both the structure and chemical nature at the organic−metal interface. In the joint theoretical and experimental paper by Hayashi et al., for instance, the intensity and energy position of vibrational modes in the HREEL spectrum of the methylthiolate/Au(111) system have been compared with their theoretically calculated counterpart, obtaining important information on the molecular adsorption site and orientation.[46] In the case of S-bonded adsorbates on metal surfaces, important clues on the strength of the interface bonding can be derived from the S−metal stretching mode. For chemisorbed thiolate on gold surfaces, the S−Au stretching mode is known to lay at 30 meV.[37,46,47] Here, vibrational properties of the low-temperature DMDS layer, and their evolution as a function of annealing temperature, are measured by means of HREEL spectroscopy, as compared with those of the MT layer. The HREEL spectrum of the MT monolayer (obtained by dosing DMDS at room temperature) is reported in the upper curve of Figure 2. The most intense feature of the spectrum is the S−Au stretching mode at 30 meV. Weaker features of the MT spectrum are observed at 117, 162, 175, 362, and 370 meV (943, 1306, 1411, 2919, and 2984 cm^{-1}) and are attributed to C−H bending, symmetric, and asymmetric deformation and stretching modes, respectively.[37,46] The HREEL spectrum of the DMDS layer, obtained by dosing DMDS at 100 K, is reported in the lower curve of Figure 2. Here, only a small peak can be observed at 30 meV, while the largest peak, which is not present in the MT spectrum, is located at 16 meV. In contrast, the remaining bands at higher frequency are very similar to those of the MT layer, with no additional peaks. Upon annealing to 250 K, the 16 meV peak disappears, transforming into the 30 meV thiolate S−Au peak (see Figure 2). We therefore associate the 16 meV feature to the S−Au stretching

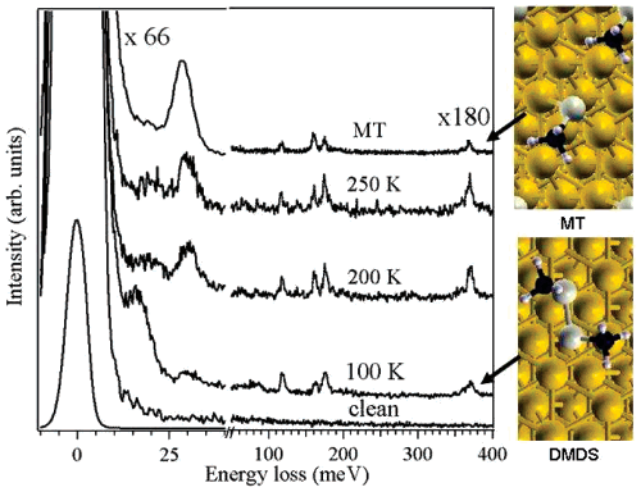

Figure 2. HREEL spectra of DMDS as a function of annealing temperature. MT spectrum is also shown (upper curve). Spectra were taken in specular geometry ($\theta_{in} = \theta_{out} = 60°$), with primary beam energy of 4.2 eV and energy resolution better than 6 meV. Inset shows the calculated binding geometries of DMDS and MT obtained from DFT simulations.

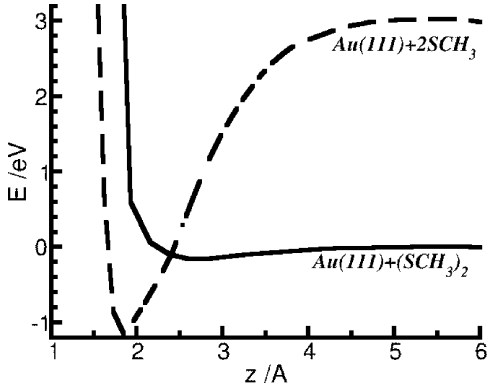

Figure 3. Calculated binding energy curves for DMDS (solid line) and MT (dashed line) as a function of the distance, *z*, from the Au surface. Energy is with respect to 1 mol of DMDS in the gas phase, and the minimum energy structure of each layer was employed, ie., DMDS-1 and MT/bridge; see text for details.

mode of the DMDS adsorbed layer, while the small 30 meV peak observed at LT is attributed to a small fraction of already dissociated molecules. The red-shift of the S−Au stretching mode of DMDS layer, relative to that of MT, indicates that the S−Au interaction in the former is weaker than in the latter. This finding is further confirmed by XPS core level measurements, as discussed in the following section. A similar red-shift, from 30 to 25 meV, has been recently reported by Noh et al.[51] in the case of dioctaldecyl sulfide ($(C_{18}H_{37})_2S$, DOS) adsorption on Au(111) and has also been attributed to the weakness of the Au−S bond in saturated compounds. It is important here to note that no clear evidence for a S−S stretching mode (expected around 66 meV) has been observed in our DMDS spectra. This is not surprising, as the intensity of this mode is expected to be very low due to its small dipole moment and to the almost flat molecular orientation. For instance, the S−S stretching mode could be detected only as a faint feature, even in the DMDS physisorbed multilayer spectra.[37] Indeed, our measurements provide first evidence that the energy value of the S−Au stretching mode is a clearer fingerprint of the existence of a weakly adsorbed disulfide species than the direct observation of a S−S vibrational mode. The high energy-loss side of the DMDS spectra does not show any dramatic change upon annealing, apart from subtle intensity rearrangements in the C−H vibrational mode features. This finding suggests that the orientation of methyl groups are similar in both DMDS and MT layers.

On the basis of HREELS measurements, we therefore identify the existence of a low-temperature weakly adsorbed DMDS layer, evolving into a high-temperature chemisorbed MT phase upon annealing. To obtain a complete picture of the properties of both phases, we performed DFT simulations on DMDS and MT layers at ratios of S/Au of 1:3, corresponding to full-coverage monolayers and considering the resulting structures and energetics. For DMDS, we find two stable minima (see Table 1), with binding energy $\approx$ 0.1−0.2 eV, both of which exhibit similar S−C tilt angles, $\theta_{tilt} = 55°$. The distinguishing features between these two minima are the number of Au−S contacts. In the lower-energy species, DMDS-1, one of the S atoms resides in an on-top site, with a 2.85 Å Au−S distance and $z_S = 2.7$ Å above the surface. In the other, DMDS-2, the S atom has moved away from the on-top position and has a nearest-neighbor contact of 3.35 Å and $z_S = 3.1$ Å. In accord with the above interpretation of the HREEL spectrum, the S−S bond in both cases is oriented almost parallel to the surface with an angle of 73° and 87° to the surface normal. The existence of multiple iso-energetic weakly bound minima is not surprising, and the DMDS results may be affected by significant uncertainties due to the lack of dispersion (van der Waals) forces within gradient-corrected DFT. However, the current findings indicate a weak Au−S interaction in accord with the HREELS results and previous theoretical studies.[22,38] To verify that these species correspond indeed to energy minima, we have calculated a binding energy curve, see Figure 3, by rigidly translating the DMDS molecule in the direction of the surface normal. For both structures, in agreement with HREELS results, a well-defined but shallow minimum energy basin was obtained that was relatively broad, with heights of DMDS between 2.6 and 3.5 Å being essentially iso-energetic. DFT does therefore find a shallow minimum for weakly adsorbed DMDS in accord with experimental observation, although the strength of the binding is underestimated and there is a large uncertainty in the relative height of the DMDS molecule from the surface. Simulations of MT/Au(111) place the lowest-energy configuration of the thiolate at a bridge site, slightly displaced toward the fcc hollow by 0.2 Å (see Figure 2). The binding energy of 1.1 eV relative to gas-phase DMDS, see Table 1, is in agreement with the experimentally measured thermal desorption energy of 1.3 eV,[52] as well as previous theoretical studies.[38,46] The structure is characterized by the S atom residing $\approx$2.0 Å above the Au surface. The observed $\theta_{tilt} = 54°$ is similar to that observed in DMDS, which is in accord with the interpretation of the intensity trends observed in the HREELS. In passing, both the fcc hollow site and on-top (see Table 1) site provide binding energies far lower than experiment. Moreover, it is important to note that ref 46 also demonstrates that the bridge site quantitatively reproduces the HREEL spectrum. The calculated binding energy curve (Figure 3) shows a well-defined minimum, with energy of 1.1 eV lower than gas-phase DMDS and a clean Au surface and a 2.8 eV dissociation energy limit corresponding to the energy required to break the S−S bond of DMDS to form 2 MT radicals. Finally, there is no barrier between the dissociated MT and the chemisorbed state, which indicates that there is no weakly adsorbed state of the MT radical. Taken together, the HREELS spectra and our detailed simulations of the structure present the following bonding scenario. At $T < 150$ K, DMDS weakly adsorbs to Au(111), where it forms a metastable surface

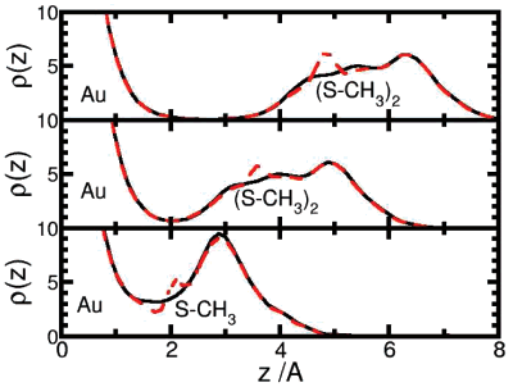

Figure 4. Calculated *z* projection of the valence electron densities from DMDS and MT at the Au surface for the ground state (solid) and with a S 2p core hole (dashed): (upper panel) DMDS $z_S = 4.2$ Å; (middle panel) DMDS $z_S = 3.0$ Å, i.e., the configuration of weakly adsorbed state; (lower panel) MT in the bridge binding configuration.

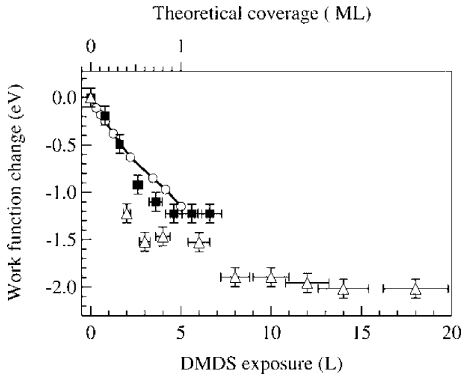

Figure 5. Comparison of $\Delta\Phi$ as a function of dosage for DMDS deposition at $T = 100$ K (open triangles) and room temperature, to form MT phase (filled square). A comparison based solely upon the calculated MT molecular dipole layer as a function of coverage (open circle) is also given.

layer. Upon heating, there is sufficient energy to rupture the S−S bond of DMDS to form two chemisorbed MT molecules.

B. Electronic Properties. *1. Core Level Photoemission.* The proposed binding scenario is confirmed by the evolution of the binding energy of the S 2p core level, as measured by XPS. The S $2p_{1/2}$ core level peak of the $T = 100$ K DMDS layer is found at 163.8 eV, a value typical of thiol and disulfide molecules weakly adsorbed (i.e., not chemisorbed) to the surface.[53] In concurrence with the appearance of the HREELS peak at 30 meV, upon annealing, the S 2p core level binding energy shifts to 162.0 eV, a value typical of chemisorbed thiolate layers.[53] Thus XPS data provide further strong evidence for our assignment of a weakly adsorbed phase of DMDS at low temperature, which evolves into MT upon annealing above 200 K.

To further validate our theoretical picture, as well as gain some initial insights into the nature of the interfacial electronic structure, we have investigated the S 2p core hole spectra by the use of an effective core hole pseudopotential for S.[50] Using only the unrelaxed valence electron wave functions provides almost identical core level energies for both DMDS and MT, see Table 1. This measure of the initial-state energy reflects the fact that the charge state of S is identical in all these materials and that the experimentally observed 1.8 eV shift between DMDS and MT layers does not result from a charge transfer from Au to MT upon chemisorption. Relaxing the valence electrons to take into account final-state effects shows only a small variation (0.0 and −0.4 eV for DMDS-1 and DMDS-2, respectively) in the binding energy of the two DMDS structures, whereas the MT bridge and on-top geometries show a reduction of the binding energy of 2.0−2.5 eV relative to these weakly adsorbed states. On the other hand, our calculations do indicate that the MT fcc hollow site provides only a 0.6−1.0 eV reduction. Hence, the observed core hole spectra may be explained by a final-state effect related to the partial screening of the S 2p core hole by the valence electrons. To understand this process in greater detail, we present in Figure 4 the *z* projection of the valence electron density for selected configurations of DMDS and MT at the Au surface. For a DMDS molecule that is located 4.2 Å above the Au(111) surface, i.e., outside the van der Waals contact distance, the calculated final-state core hole moves to slightly lower binding energies (−0.3 eV lower) with respect to the weakly adsorbed DMDS. By comparing the density of the ground state and the final "core hole" state, one sees that there is a density pile up about the S atom with a corresponding decrease in density around the S lone pairs and S−C bond. In the weakly adsorbed state of DMDS, this effect is also present but somewhat mitigated by the density tail from the Au surface. However, for the MT bound at the bridge configuration, the majority of the density employed to screen the core hole comes from the Au−S bonding region. Thus, our simulations suggest that the observed core hole energy shifts are a final-state effect, which results from different core hole screening mechanisms operative for the weakly adsorbed DMDS and chemisorbed MT layers. This qualitatively explains why the fcc site, which is farthest from the Au atoms and bound in a low electron density area, exhibits a small core hole shift.

Our experimental XPS results do corroborate unambiguously our picture of a low-temperature weakly adsorbed DMDS layer and high-temperature chemisorbed MT phase as observed with HREELS. The theoretical simulations of the XPS S 2p core hole spectra support the experimental interpretation, with the important observation that the charge state of S in both weakly adsorbed DMDS and MT are essentially identical.

2. Work Function. We next report on the influence of the nature of molecule−metal interaction on the system work function, Φ, as measured by UPS. Relative to the clean Au surface, Φ decreases by −1.2 eV upon deposition of a full MT monolayer at room temperature (corresponding to ∼5 L exposure, see Figure 5). For DMDS deposition, the $\Delta\Phi$ variation with exposure reaches a plateau around −1.5 eV and then saturates at −2.0 eV. The first plateau corresponds to a coverage region between 0.6 and 1 ML (as estimated by XPS), while the saturation is reached with the formation of a physisorbed multilayer (as indicated by UPS valence band measurements). In Figure 6, right axis, we show the evolution of $\Delta\Phi$ for the DMDS layer upon annealing. The $\Delta\Phi$ initial value for DMDS (0.6 ML coverage) is −1.2 eV at 110 K and progressively reduces, reaching the value of −0.8 eV around 250 K. Such a reduction cannot be attributed to desorption processes, which are ruled out by the constant value of the S 2p XPS peak intensity. We therefore attribute these changes to the chemical modification of the interface, as induced by the dissociation of DMDS into chemisorbed MT.

For a direct comparison with experiment, we consider the calculated V_{ES} for Au(111) with and without the molecular adsorbates (see Figure 7). The clean Au(111) surface reproduces the experimental value of $\Phi_{Au} = 5.35$ eV,[54] giving us confidence in the reliability of our approach.

The theoretical simulations can quantitatively account for the observed negative $\Delta\Phi$ values. For the MT phase, $\Delta\Phi = -1.2$ eV for the bridge structure at full coverage, in agreement with

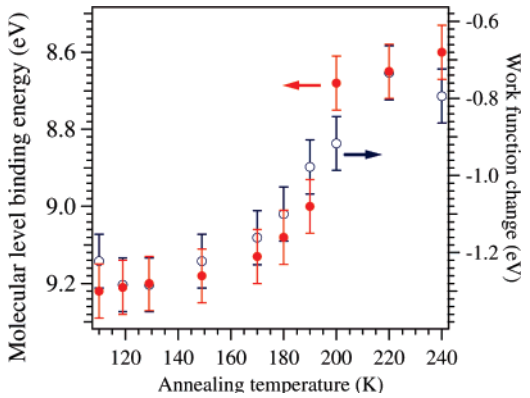

Figure 6. Change of $\Delta\Phi$ (right axis, empty symbols) and of M-state energy level (left axis, filled symbols) upon annealing of 0.6 ML DMDS.

the experimental values in Figure 5. By referring to Table 1, it can be seen that the fcc site also provides a satisfactory estimate of $\Delta\Phi = 1.1$ eV, whereas the on-top site clearly underestimates the experimental result. Given that the bridge site is the only configuration that also explains all the other experimental data, we confine further discussion to calculations assuming an adsorbate structure with this configuration. Hence, we find that, at half coverage, a structure consisting of bridge sites provides $\Delta\Phi = -0.8$ eV, in excellent accord with the experimentally observed $\Delta\Phi = -0.8$ eV at 0.6 ML. For DMDS at half coverage, $\Delta\Phi = -1.0$ eV, which is lower than the MT phase by 0.2 eV, matching the experimental trend but underestimating the magnitude by 0.2 eV. Adjusting the height of the DMDS molecule by translating it 0.5 Å closer to the surface does not alter $\Delta\Phi$. This demonstrates that errors in the binding geometry, as a result of the lack of dispersion forces within DFT, do not influence the work function results significantly and suggests that the underestimation comes from the approximation of the film morphology as homogeneous. Moreover, at low temperature, it is not possible to obtain experimentally a complete DMDS monolayer before starting to grow successive physisorbed layers. We therefore cannot directly compare the theoretical value of $\Delta\Phi$ of the full DMDS monolayer with the corresponding experimental value. Nevertheless, an extrapolation for the full monolayer can be obtained from the coverage dependence of $\Delta\Phi$ (see Figure 5), leading to a value between -1.5 and -1.9 eV, which matches the theoretical $\Delta\Phi = -1.6$ eV, as obtained from both weakly adsorbed DMDS configurations.

To understand the origin of the observed $\Delta\Phi$, we construct a surface dipole potential by considering the difference between V_{ES} of the total system and the sum of the potentials obtained from the isolated surface slab and molecular layer. For MT/Au(111), V_{ES} is almost exactly the sum of that for a neutral MT layer and a Au(111) surface with at most a 0.05 eV contribution from charge transfer (see Figure 7). Indeed, an estimate of the amount of charge transfer, δq, can be obtained by assuming a plate-capacitor model where $\Delta V_{ES} = 4\pi\rho\delta q d = 0.05$ eV, where ρ is the density of molecules at the surface, which for a Au−thiol separation of 2.0 Å results in $\delta q \approx 0.004$ *e*. This matches qualitatively with an alternate estimate based on Bader population analysis of around 0.01 *e*. This observation, which is in full accord with our interpretation of the S 2p core hole shifts, can be understood in a simple way by considering the calculated chemical potentials (or electronegativity (EN)). Since both HOMO and LUMO orbitals of MT are located on the S atom, which is the direct point of contact between the

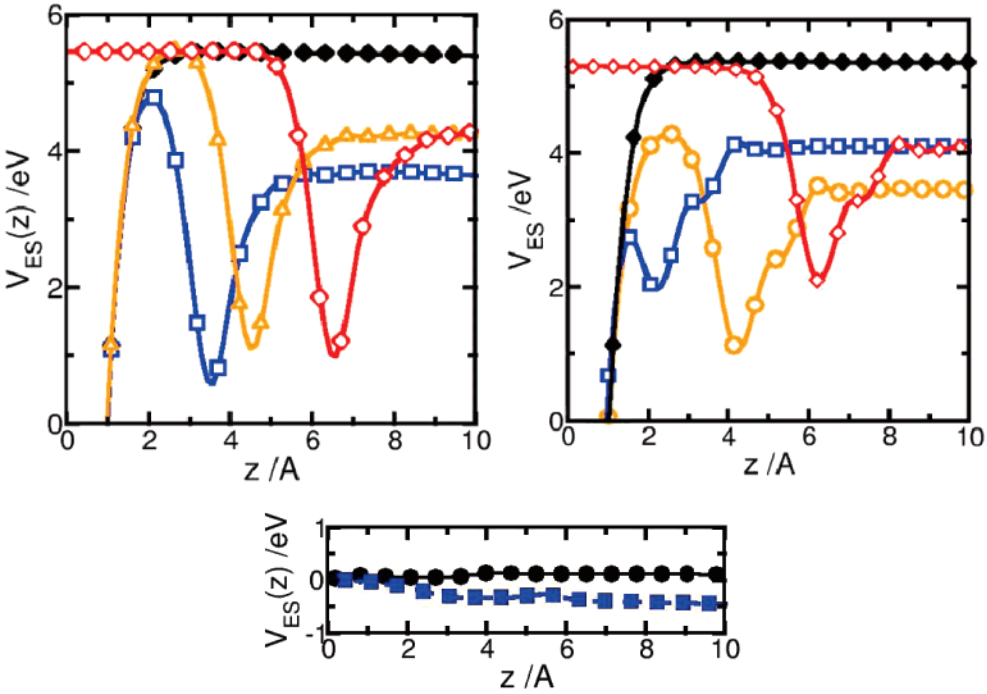

Figure 7. The *z* projection of V_{ES} for full coverage DMDS/Au(111) (top panel, left) and MT/Au(111) (top panel, right); curves are plotted such that $E_F = 0$. Top panel, left: for the DMDS-2 structure, V_{ES} is shown for the molecule located in the weakly adsorbed state, $z_S = 3.1$ Å (open squares), and at larger distances, $z_S = 4.2$ Å (open triangles). The clean Au(111) (filled diamonds) and isolated DMDS layer (open diamonds) V_{ES} are also shown. Top panel, right: for MT, V_{ES} is shown at global minimum for the bridge position $z_S = 2.0$ Å (open squares), for $z_S = 3.5$ Å (circles), clean Au(111) (filled diamonds), and isolated MT layer (open diamonds). Lower panel: the difference between V_{ES} for the adsorbed layer, DMDS-2 ($z_S = 3.1$ Å, squares), and MT ($z_s = 2.0$ Å, circles). The difference potential is calculated by subtracting from V_{ES} of the adsorbed layer the sum of the potentials obtained from the isolated molecular layer and Au(111). Note that the difference curve reveals a potential drop of 0.4−0.5 eV for DMDS, whereas for MT, there is a slight increase of less than 0.05 eV.

molecule and the surface, it is sufficient here to employ a total molecular electronegativity, whereas a local measure of this property would be required for molecules that interact with the surface by a variety of functional groups. It is found that the MT layer, like gas-phase MT, has an EN = 5.4 eV, which is almost equal to that of Au(111) (EN = 5.3 eV), thus explaining the little metal-surface-to-molecule charge transfer. $\Delta\Phi$ can be ascribed almost entirely to the dipole moment of the MT molecular layer with no significant contribution from the charge redistribution occurring during Au−thiolate bonding.

For DMDS, we find a slightly different scenario. The decomposition of V_{ES} into molecular and surface components shows the molecular dipole layers in both DMDS and MT layers to induce almost the same potential drop (see Figure 7). However, the decomposition analysis reveals a jump across the interface for the DMDS layer that accounts for the remaining 0.4 eV. This results from a shift in the electron density *toward* the surface. Considering DMDS at a slightly larger distance from the surface, $z_S = 4.2$ Å (see Figure 7), i.e., outside of the weakly bound minimum, the system shows, like the chemisorbed MT, a $\Delta\Phi$ corresponding to only a molecular dipole term. Hence, the difference between the chemisorbed and the weakly adsorbed layers is only due to a small alteration of the density at intermediate distances from the surface. The observed charge displacement is consistent with a shift of the diffuse tail of the Au surface electron density back toward the metal slab via Pauli repulsion, the so-called "pillow mechanism", with the electrons of DMDS, similar to the case of the Xe.[12,13] To probe this finding further, we have also considered the hypothetical situation where MT is located at a distance where $z_S = 3.5$ Å, i.e., a similar distance from the surface as the weakly adsorbed DMDS. The calculated V_{ES} also reveals a lower $\Delta\Phi$ by approximately −0.4 eV, more than can be accounted for by purely the molecular dipole. From this observation, we learn that: (i) A Pauli repulsion term similar to the one found for DMDS would also arise for the MT layer if it were bound at distances from the surface on the order of DMDS. (ii) The rearrangement of the electrons at the surface that occurs in chemisorption completely cancels out the Pauli repulsion effect on $\Delta\Phi$, and thus one returns to the scenario where only the molecular dipole influences the surface work function. Hence, it may be concluded that Pauli repulsion does not contribute to the lowering of metal surface work functions for this type of chemisorbed species, contrary to the findings of ref 8 for aromatics and to the assumption taken in ref 36. It is important to stress that, for both MT and DMDS systems, the major contribution to $\Delta\Phi$ arises from the molecular dipole layer. We now clarify how this molecular dipole layer relates to the permanent molecular dipole as found for individual molecules. Noting that $\Delta\Phi = 4\pi e\rho\mu\cos(\Theta_{tilt})$, where μ is the molecular dipole, it is found that the experimental values of $\Delta\Phi$ imply $\mu = 1.4$ and 1.2 D, at half and full coverage for an MT molecule in the bridge configuration. This is significantly lower than the 1.9 D value calculated from the gas-phase molecule and results from the depolarization of the molecule by its neighbors.[33] Our calculation of a molecular slab, which employs periodic boundary conditions, accounts for this depolarization field. To confirm this idea, we calculated the molecular dipole of an isolated thiolate layer as a function of layer density (i.e., coverage). We model the layer density by gradually increasing the distances between the MT molecules and calculate the estimated $\Delta\Phi$ from the drop in V_{ES}. The obtained values are compared in Figure 5 with the room-temperature experimental data, showing a remarkably good agreement. The underestimation of theoretical values relative to the experiment at intermediate coverage can be rationalized by the formation of full-coverage islands, as indicated by the presence of $(\sqrt{3} \times \sqrt{3})$ spots in the low-energy electron diffraction images at ∼0.7 ML.[55] These results demonstrate that a depolarization effect upon the molecular dipole occurs and indicates that quantitatively accounting for the observed $\Delta\Phi$ can only be accomplished by considering electrostatic interactions between the molecules in the layer and not solely by gas-phase dipoles.

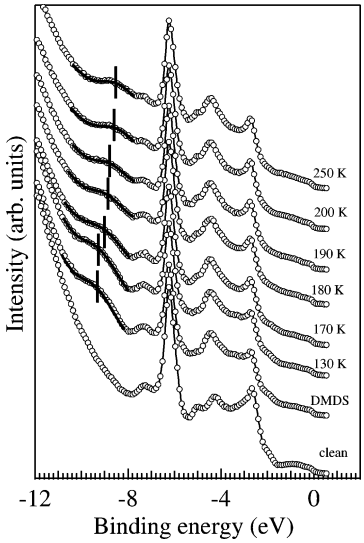

Figure 8. Temperature dependence of UPS spectrum of 3 L DMDS sample. The position of the M-state, as determined by fitting the spectra with a Gaussian peak and an exponential background, is indicated by a vertical line for each curve. The fitting curves are also shown as solid lines.

C. Molecular-Level Alignment. The MT/Au(111) system represents a simple prototypical model for the study of molecular-level alignment in this important class of interfaces. The possibility to switch from the DMDS physisorbed system to chemisorbed MT by simple annealing allows us to study in detail the modification of the electronic DOS when a chemisorbed thiolate interface is formed, starting from a weakly interacting molecular layer. Given this opportunity, two main issues can be address: (i) determine how the energy of molecular levels varies upon modification of the interface dipole layer; (ii) evaluate the modifications of the electronic DOS induced by the formation of a thiolate−metal bond with special emphasis on the modification of the HOMO states of the molecule. Both of these issues have been addressed by measuring the UPS valence band evolution of the DMDS layer as a function of annealing temperature, as shown in Figure 8, and comparison with theoretical DOS.

1. Molecular States. To address the first issue, we focus on the energy position of the broad peak observed at −9.2 eV binding energy in the DMDS valence band spectrum in Figure 8, which is attributed[56] to a molecular state primarily localized on the methyl groups, denoted as the M-state. Upon annealing to around 250 K, this feature shifts toward lower binding energy, reaching the value of −8.6 eV, which corresponds to the binding energy of the methyl-localized state in the thiolate layer. It is important here to notice that, in the case of UV photoemission from molecular states, Koopmans' theorem is not valid and final-state contributions to the observed energy of the M-state have to be taken into account.[4] Nevertheless, the local environment of the M-state can be safely considered to be the same for both MT and DMDS systems. We can therefore reasonably assume

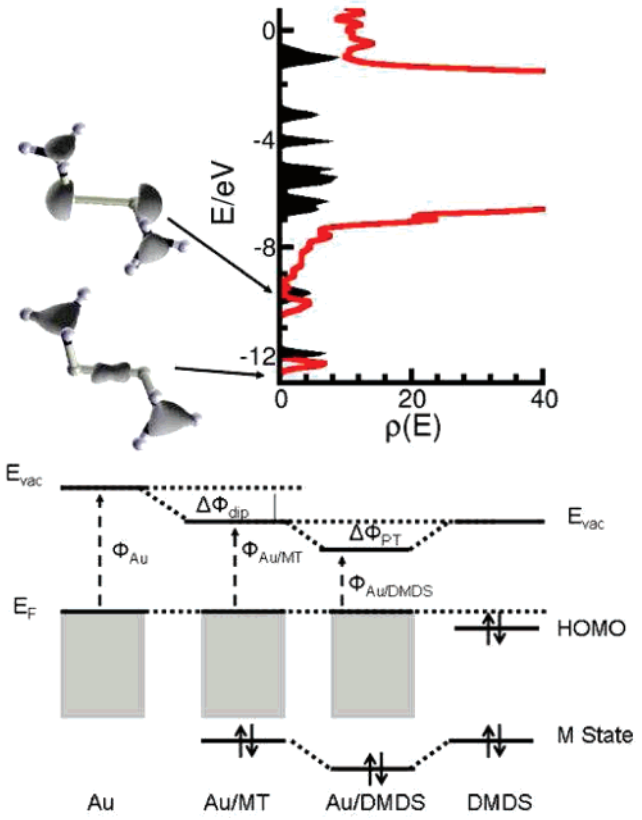

Figure 9. Upper panel shows the calculated electronic DOS for an isolated DMDS layer (shaded black) and in the weakly adsorbed state (red). Lower panel shows the schematic of alignment of E_{vac} and the M-states for the isolated DMDS layer, weakly adsorbed DMDS, and chemisorbed MT.

the final-state contribution to the observed M-state energy to be the same for both MT and DMDS and attribute the shift in the M-state position in the UPS spectra only to changes in its initial-state binding energy. In Figure 6, the molecular-state binding energy evolution as a function of temperature (0.6 ML coverage) is reported and compared with the corresponding $\Delta\Phi$. These data demonstrate, in agreement with the picture described by Kahn,[4] that the interface dipole layer formed by the redistribution of charge density occurring on passing from weakly adsorbed to chemisorbed phase affects the electron-level alignment and the work function in the same way and that even small density rearrangements at the interface can have nonnegligible effects on the electron level alignment.

To understand these observations theoretically, yet avoiding difficulties arising from the splitting of MT states when two molecules are combined to form DMDS, we pursue an alternate-but-complementary strategy. Here, we consider how the M-state orbitals of the DMDS layer are shifted as it is brought into contact with the surface. Because of final-state effects discussed above, a quantitative comparison between experiment and theory is not possible. However, the shifts in the energy level may be evaluated. To do this, we consider the DOS of an isolated DMDS layer as compared with that of the weakly adsorbed DMDS layer (see Figure 9). Qualitatively, the DOS of the adsorbed layer has similar features to the UPS spectrum in Figure 8; the Au d-band dominates both the DOS and the UPS spectrum between −8 and −2 eV, while below −9 eV are well-localized states on the molecules (see upper panel in Figure 9 for isosurface plots of the relevant orbitals). The DOS for the DMDS layer (shaded curve in Figure 9) shows sharp peaks typical of flat bands of an insulating molecular layer. By comparing this DOS with that of the adsorbed layer, it can be seen that, for the molecular states below the Au d-band, there is almost a direct mapping onto those of the layer with a uniform shift of 0.4 eV. Visual inspection of the wave functions of these states for the adsorbed DMDS indicates that they are identical with those of the isolated molecular layer. These observations can be understood in terms of the V_{ES} of the DMDS layer, see Figure 7, which for $z_S > 2.5$ Å is similar to that of the isolated layer except for a downward energy shift arising from the dipole potential caused by Pauli repulsion with the electrons of the Au surface. This result is in accord with the experimental observation and may be understood as arising from the fact that, for adsorbed DMDS, the M-states are noninteracting with the surface. Thus, these states are anchored to a fixed vacuum level such that the observed change of their energy position in UPS measurements are to be ascribed solely to changes in the position of E_F with respect to the vacuum level. This scenario is illustrated schematically in the lower panel of Figure 9 and is in agreement with the experimental interpretation.

2. Interface States. To address the second issue noted above, we first need to briefly recall the News−Anderson model for adsorbate−metal bonding,[57] according to which the sulfur p orbitals (which correspond to the molecular HOMO) couple to the metal orbitals, giving rise to bonding and antibonding peaks. This bonding mechanism has been theoretically studied in the case of cysteine adsorption on Au(111),[58] while several thiolate/Cu interfaces have been studied both experimentally and theoretically[56,59] and at the semiempirical level[60] for alkanethiolates on Au(111). Hence, we perform a similar analysis of the modification of the theoretical DOS and UPS on passing from the DMDS to the MT layer to allow us to gain more insight into this topic. The modification of the valence band spectra in the [−8, 0] eV binding energy region are quite subtle and can be best analyzed by considering the difference spectra between the MT and DMDS layers, respectively, and the clean Au(111) surface. Unfortunately, there is no unequivocal criterion for spectrum normalization prior to subtraction, as all features of the clean valence band spectrum are in principle affected by the adsorption process. We have therefore considered two different ways of subtracting spectra, i.e., (i) subtraction of raw data without normalization (corresponding to the hypothesis of perfect reproducibility of experimental conditions and negligible bulk-Au state intensity attenuation), and (ii) normalization of spectra to the Fermi edge intensity based on the theoretical result that almost no change in the DOS is expected *at the Fermi level* (see below). The normalization constant in the two procedure differs by less than 20% so that the main features of the difference spectra do not depend significantly on the chosen normalization. In the following, we therefore restrict our discussion to these main features, displaying for simplicity in Figure 10 only the E_F-normalized difference spectra (DMDS-clean, MT-clean, and MT-DMDS). Both DMDS and MT experimental difference spectra are characterized by an intensity increase in the [-2, 0] eV and [−6, −3] eV energy regions and a decrease in the [−2, −3] eV region. However, the relative intensities differ significantly between DMDS-clean and MT-clean, as is best evidenced in the MT-DMDS difference spectrum in Figure 10. Between 0 and −2 eV and for all normalization, the DMDS-clean spectrum shows a broad feature centered around −1.5 eV, whereas the MT-clean spectrum shows a larger intensity with a peaked maximum slightly shifted toward the Fermi level. Analogously, the spectral increase in the [−3, −6] eV region is more pronounced in the MT-clean spectrum than in the DMDS one for all normalizations. The

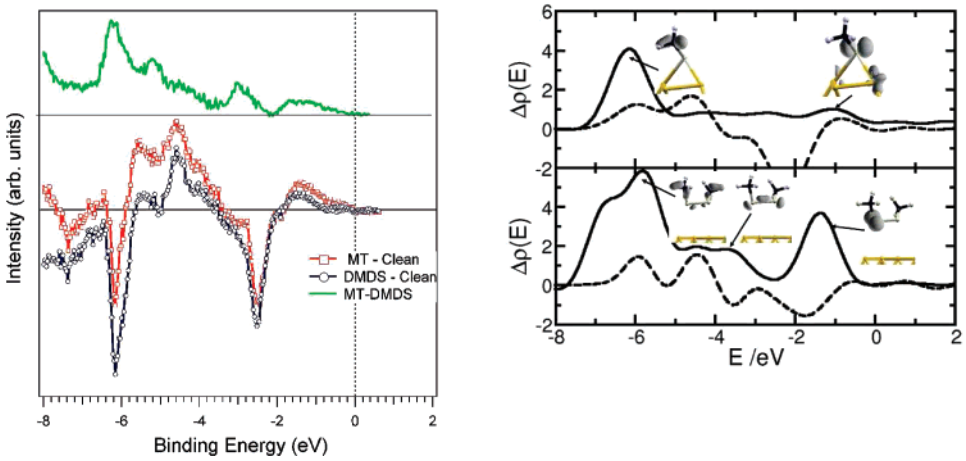

Figure 10. Left panel shows the difference in the UPS spectrum MT/Au(111) and clean Au(111) at 250 K (MT-clean, squares), weakly adsorbed DMDS/Au(111) at 110 K, and clean Au(111) (DMDS-clean, circles), and the same sample at 110 and 250 K (MT-DMDS, solid line). Right panel: the corresponding difference between the calculated partial DOS are shown for MT-clean (upper subpanel) and DMDS-clean (lower subpanel). Projections are included only for thiolate layer (solid line) and d orbitals of surface Au atoms (dashed line). To characterize the relevant states associated with the various features in the difference curves, selected orbital density plots (for the Γ point) are included as insets. Calculations are performed with the PWSCF code with a Gaussian broadening of the DOS of 0.05 eV.

depletion of UPS intensity just below −2 eV is also observed in both difference curves with almost the same intensity (although in this region, a quantitative comparison is made difficult due to the uncertainty in the normalization procedure). A direct *quantitative* comparison with our simulations is not possible due to final state effects and lack of Au spin−orbit contributions in our scalar relativistic approach. Moreover, the UPS excitation wavelength allows for photoemission from only 3−4 atomic layers from the surface; hence, we focus our attention on the partial DOS of the chemically relevant atoms as opposed to the total DOS of the entire surface slab. For a *qualitative* comparison, we consider the partial DOS of the surface Au atoms and the molecular layer as calculated by projecting the wave functions onto a minimal localized basis set consisting of the atomic pseudo-orbitals associated with each potential. Note that the total DOS is reproduced to greater than 99% by a sum of the projections on all the orbitals in our basis, ensuring the completeness of our description. Specifically, we consider the partial DOS arising from the adsorbed MT/DMDS molecular layer and the Au atoms directly at the surface, which only show significant changes in their atomic d-orbital population. These projections are plotted in Figure 10, along with some of the representative orbital densities as isosurfaces. Figure 10 shows that the DOS changes at the Fermi level are very small for both systems, thus supporting the proposed E_F normalization of the experimental spectra. Indeed, in the case of the MT layer, a small decrease of the empty-state DOS just above the Fermi level is observed, which indicates a chemisorption-induced depletion of the Au d-holes. The theoretical results for the MT layer assign the intensity increase below E_F to the presence of Au−S antibonding orbitals arising from the formation of a Au−S bond, in accord with the News−Anderson model.[57] The experimentally observed depletion of the UPS intensity just below −2 eV is also in qualitative agreement with our calculation and results from the remixing of Au d orbitals of the surface atoms upon adsorption of the molecule. Upon remixing, the Au d orbitals are shifted from the [−4, −2] eV region of the DOS to [−6, −4] eV, thus explaining the experimental intensity increase in this region, which corresponds to the bonding state in the News−Anderson model. In this region, a contribution from states localized on the MT molecules is also detected, and in particular, the UPS intensity observed just above −6 eV derives from both C−H and C−S orbitals. As shown in the isosurface plot of Figure 10, the MT molecular orbitals involved in the bonding are strongly coupled with orbitals in the bulk, hence decreasing their net contribution to the intensity at any given energy. For the DMDS layer, the intensity increase in the [0, −2] eV region is mainly due to the nonbonding S orbitals at −2 eV, although a component due to Au DOS rearrangement is also present. Indeed, in the whole [0, −6] eV region, the Au DOS variations of the weakly adsorbed DMDS system are quite similar, though less pronounced, to those observed for the MT layer. In particular, the observed UPS intensity depletion around −2 eV and increase in the [−3, −6] eV region of the DMDS layer are associated with variations in the Au DOS. These variations are of course larger for the MT-clean system than for the DMDS-clean, indicating that a stronger density of state rearrangement occurs upon formation of the chemisorption bond. Moreover, the intensity increase in the [−3, −6] eV region of the DMDS layer is also partially due to the presence of DMDS molecular orbitals with C−S and C−H character.

It is interesting to note that all DMDS molecular states are well localized (i.e., have flat bands), and their energy positions can be directly derived by those of the corresponding states in the isolated DMDS layer (see Figure 9) with a rigid shift by −0.4 eV, i.e., all DMDS states behave as the M-state. On the contrary, for the MT layer, the energy positions of all the molecular levels around E_F that are involved in the bonding and, in particular, of the antibonding S−Au orbital that corresponds to the HOMO level, are determined by the detail of the bond formation and cannot be directly linked with the vacuum-level alignment, i.e., with work function variations. In summary, the investigation of the UPS and valence electron DOS provides a complementary picture with that obtained from our analysis of XPS and work function measurements. Upon annealing, the DMDS layer there is a strong rearrangement of the states below E_F caused by the formation of an Au−S contact. This fits well with a News−Anderson model, and our calculations predict, for the chemisorbed layer, MT states just above E_F accompanied by depletion of Au-*d* hole states. This last observation nicely matches the recent interpretation of X-ray near-edge spectroscopic measurements performed on large Au−thiol nanoparticles.[61]

IV. Conclusions

Our combination of HREELS, XPS, UPS measurement, and DFT simulations of DMDS and MT SAMS on Au(111) has allowed us to evolve a detailed and consistent picture of the bonding between weakly adsorbed disulfides and chemisorbed thiols on gold surfaces. We find that the interfacial electrostatics as observed in XPS and UPS are entirely consistent with a picture of methylthiolate radicals covalently bound to Au with essentially no metal−molecule charge transfer. Our results corroborate the observation of a decrease in hole states in the Au−S band upon thiolate adsorption linked with magnetism in Au−thiol nanoparticles[61] but does not support the large charge transfer required for the proposed mechanism for magnetism at Au−thiol interfaces.[32,34] It is our firm belief that significant further investigation into the underlying mechanism of the apparent giant magnetic behavior of these films is necessary to clarify these issues. Instead, the main ingredient of the surface dipole layer is the permanent molecular dipole and places previous indirect observations from the literature[35,36] on a firmer foundation. Noting that controversy does surround the actual structure of MT/Au(111),[63] our current results suggest that, regardless of the coordination site of S, the primary structural feature responsible for the interfacial electrostatics is Θ_{tilt}, which should be about 55°. Our results also suggest that there should be little dependence of the electrostatic properties of this interface on the exact phase of the monolayer. Theoretical predictions on the superstructure of the monolayer, c(4 × 2)[38,62] and (3 × 4),[55] indicate that these phases consist of inequivalent bridge sites or a mixture of bridge and on-top sites with similar densities and Θ_{tilt} as the ($\sqrt{3} \times \sqrt{3}$) *R*30° structure and hence should have similar electrostatic profiles. Moreover, UPS measurements indicate that the work function of the (3 × 4) and of the ($\sqrt{3} \times \sqrt{3}$) *R*30° structures are identical within the experimental error.

Finally, our study clarifies the role of molecular-dipole, charge-transfer, and Pauli repulsion at these interfaces, which should allow for better analysis and control when designing Au(111)−thiol systems with specific interfacial electrostatic properties.

Acknowledgment. We acknowledge partial support from INFM through "Parallel Computing Initiative", and from MIUR through PRIN 2003 and FIRB NOMADE. We thank L. Casalis, A. Morgante, G. Scoles, A. Dal Corso, and E. Tosatti for discussions.

References and Notes

(1) Cui, X. D.; Primak, A.; Zarate, X.; Tomfohr, J.; Sankey, O. F.; Lindsay, S. M. *Science* **2001**, *294*, 571−574.

(2) Seltzer, Y.; Salomon, A.; Cahen, D. *J. Phys. Chem B* **2002**, *106*, 10432−10439.

(3) Scott, J. C. *J. Vac. Sci. Technol., A* **2003**, *21*, 512−531.

(4) Kahn, A.; Koch, N.; Gao, W. Y. *J. Polym. Sci., Part B: Polym. Phys.* **2003**, *41*, 2529−2548. Cohen, D.; Kahn, A. *Adv. Mater.* **2003**, *15*, 271−277.

(5) Ishii, H.; Seki, K. In *Conjugated Polymer and Molecular Interfaces*; Salaneck, W. R., Seki, K., Kahn, A., Pireaux, J.-J., Eds.; Marcel Dekker: New York, 2002; p 293. Ishii, H.; Sugiyama, K.; Ito E.; Seki, K. *Adv. Mater.* **1998**, *11*, 605−625.

(6) Ashkenasy, G.; Cahen, D.; Cohen, R.; Shanzer, A.; Vilan A. *Acc. Chem. Res.* **2002**, *35*, 121−128.

(7) Zhu, X. Y. *Annu. Rev. Phys. Chem.* **2002**, *53*, 221−247.

(8) Crispin, X.; Geskin, V.: Crispin, A,; Cornil, J.; Lazzaroni, R.; Salaneck, W. R.; Bredas, J. L. *J. Am. Chem. Soc.* **2002**, *124*, 8131−8141.

(9) Cahen, D.; Kahn, A.; Umbach, E. *Mater. Today* **2005**, *8*, 32−41.

(10) Tung, R. T. *Mater. Scie. Eng. R* **2001**, *35*, 1−138.

(11) Bagus, P. S.; Hermann, K. S.; Wóll, C. *J. Chem. Phys.* **2005**, *123*, 184109.

(12) Bagus, P. S.; Steamler, V.; C. Wöll, C. *Phys. Rev. Lett.* **2002**, *89*, 096104.

(13) Da Silva, J. L. F.; Stampfl, C.; Scheffler M. *Phys. Rev. Lett.* **2003**, *90*, 066104.

(14) Hill, I. G.; Milliron, D.; Schwartz, J.; Kahn, A. *Appl. Surf. Sci.* **2000** *166*, 354−362.

(15) Shen, C.; Kahn, A.; Schwartz, J. *J. Appl. Phys.* **2001**, *89*, 449−459.

(16) Chkoda, L.; Heske, C.; Sokolowski, M.; Umbach, E. *Appl. Phys. Lett.* **2000**, *77*, 1093−1095.

(17) Ulman, A. *Chem. Rev.* **1996**, *96*, 1533−1554.

(18) See, for example: Zhou, C.; Deshpande, M. R.; Reed, M. A.; Tour, J. M. *Appl. Phys. Lett.* **1997**, *71*, 611−613. Reed, M. A.; Chen, J.; Rawlett, A. M.; Price, D. W.; Tour, J. M. *Appl. Phys. Lett.* **2001**, *78*, 3735−3737. Reichert, J.; Ochs, R.; Beckmann, D.; Weber, H. B.; Mayor, M.; von Löhneysen, H. *Phys. Rev. Lett.* **2002**, *88*, 176804. Halik, M.; Klauk, H.; Zschieschang, U.; Schmid, G.; Dehm, C.; Schütz, M.; Maisch, S.; Effenberger, F.; Brunnbauer, M.; Stellacci, F. *Nature* **2004**, *431*, 963−966. Piccini, S.; Selloni, A.; Scandolo, S.; Car, R.; Scoles, G., *J. Chem. Phys.* **2003**, *119*, 6729−6735.

(19) Schreiber, F. *J. Phys.: Condens. Matter* **2004**, *16*, R881−R900. Schreiber, F. *Prog. Surf. Sci.* **2000**, *65*, 151.

(20) Yang, G.; Liu, G.-Y. *J. Phys. Chem. B* **2003**, *107*, 8746−8759.

(21) Sellers, H.; Ulman, A.; Shnidman, Y.; Eilers, J. E. *J. Am. Chem. Soc.* **1993**, *115*, 9389−9401.

(22) Gronbeck, H.; Curioni, A.; Andreoni, W., *J. Am. Chem. Soc*. **2000**, *122*, 3839−3842.

(23) Beardmore, K. M.; Kress J. D.; Gronbeck-Jenson, N.; Bishop, A. R. *Chem. Phys. Lett.* **1998**, *286*, 40−45.

(24) Hakkinen, H.; Barnett, R. N.; Landman, U. *Phys. Rev. Lett.* **1999**, *82*, 3264−3267. Garzon, I. L.; Rovira, C.; Michaelian, K.; Beltran, M. R.; Ordejon, P.; Junquera, J.; Sanchez-Portal, D.; Artacho, E.; Soler, J. M. *Phys. Rev. Lett.* **2000**, *85*, 5250−5251.

(25) Gottschalck, J.; Hammer, B. *J. Chem. Phys.* **2002**, *116*, 784−790. Molina, L. M.; Hammer, B. *Chem. Phys. Lett.* **2002**, *360*, 264−271.

(26) Krüger, D.; Fuchs, H.; Rousseau, R.; Marx, D.; Parrinello, M. *J. Chem. Phys.* **2001**, *115*, 4776−4786. Rousseau, R.; Mazzarello, R.; Scandolo, S. *ChemPhysChem* **2005**, *6*, 1756−1760.

(27) De Renzi, V.; Rousseau, R.; Marchetto, D.; Biagi, R.; Scandolo, S.; del Pennino, U. *Phys. Rev. Lett.* **2005**, *95*, 046804.

(28) Konôpka, M.; Rousseau, R.; ×b3Tich, I.; Marx, D. *J. Am. Chem. Soc.* **2004**, *126*, 12103−12111; *Phys. Rev. Lett.* **2005**, *95*, 096102.

(29) Basch, H.; Ratner, M. A. *J. Chem. Phys.* **2003**, *119*, 11926−11942; *J. Chem. Phys.* **2004**, *120*, 5771−5780.

(30) Cometto, F. P.; Paredes-Olivera, P.; Macagno, V. A.; Patrito, E. M. *J. Phys. Chem. B* **2005**, *109*, 21737−21748.

(31) Bilic, A.; Reimers, J. R.; Hush, N. S. *J. Chem. Phys.* **2005**, *122*, 094708.

(32) Carmell, J.; Leitus, G.; Naaman, R.; Reich, S.; Vager, Z. *J. Chem. Phys.* **2003**, *118*, 10372−10375.

(33) Cahen, D.; Naaman, R.; Vager Z. *Adv. Funct. Mater.* **2006**, *15*, 1571−1578.

(34) L'vov, V. S.; Naaman, R.; Tiberkevich, V.; Vager Z. *Chem. Phys. Lett.* **2003**, *381*, 650−653. Vager Z.; Naaman, R. *Phys. Rev. Lett.* **2004**, *92*, 087205. See also: Hernando, A.; Garcia, M. A. *Phys. Rev. Lett.* **2006**, *96*, 029703. Vager Z.; Naaman, R. *Phys. Rev. Lett.* **2006**, *96*, 029704.

(35) Bruening, M.; Cohen, R.; Guillemoles, J. F.; Moav, T.; Libman, J.; Shanzer, A.; Cahen, D. *J. Am. Chem. Soc.* **1997**, *119*, 5720−5728.

(36) Alloway, D. M.; Hofmann, M.; Smith, D. L.; Gruhn, N. E.; Graham, A. L.; Colorado, R.; Wysocki, V. H.; Lee, T. R.; Lee, P. A.; Armstrong, N. R. *J. Phys. Chem. B* **2003** *107*, 11690−11699.

(37) Nuzzo, R. G.; Zegarski, B. R.; Dubois, L. H. *J. Am. Chem. Soc.* **1987**, *109*, 733−740.

(38) Vargas, M. C.; Giannozzi, P.; Selloni, A.; Scoles, G. *J. Phys. Chem. B* **2001**, *105*, 9509−9513.

(39) Perdew, J. P.; Burke, K.; Ernzerhof, M. *Phys. Rev. Lett.* **1996**, *77*, 3865−3868.

(40) Hartwigsen, C.; Goedecker, S.; Hutter, J. *Phys. Rev. B* **1999**, *58*, 3641−3662.

(41) Troullier, N.; Martins, J. L. *Phys. Rev. B* **1991**, *43*, 1993−2006.

(42) Alavi, A.; Kohanoff, J.; Parrinello, M.; Frenkel, D. *Phys. Rev. Lett.* **1994**, *73*, 2599−2602.

(43) CPMD, V3.9 Copyright IBM Corp. 1990−2001, Copyright MPI für Festkoerperforschung Stuttgart 1997−2001.

(44) Baroni, S.; de Gironcoli, S.; Dal Corso, A.; Giannozzi, P. PWSCF, version 2. See www.pwscf.org.

(45) Vanderbilt, D. *Phys. Rev. B* **1990**, *41*, 7892−7895.

(46) Hayashi, T.; Morikawa, Y.; Nozoye, H. *J. Chem. Phys.* **2001**, *114*, 7615−7621.

(47) Duwetz, A. S. *J. Electron. Spectrosc. Relat. Phenom.* **2004**, *134*, 97138.

(48) Monkhorst, H. J.; Pack, J. D. *Phys. Rev. B* **1976**, *13*, 5188−5192.

(49) Marx D.; Hutter J. In *Modern Methods and Algorithms of Quantum Chemistry*; Grotendorst, J., Ed.; NIC, FZ Jülich: Jülich, 2000; pp 301−449.

(50) Pasquarello, A.; Hybersten, M. S.; Car, R. *Phys. Rev. Lett.* **1995**, *74*, 1024−1027; *Phys. Rev. B* **1996**, *53*, 10942−10950.

(51) Noh, J.; Hara, M. *Langmuir* **2000**, *16*, 2045−2048.

(52) Danisman, M. F.; Casalis, L.; Bracco, G.; Scoles, G. *J. Phys. Chem.* **2002**, *106*, 11771−11777.

(53) Castner, D. G.; Hinds, K.; Grainger, D. W. *Langmuir* **1996**, *12*, 5083−5086.

(54) Lide, D. R. *CRC Handbook of Physics and Chemistry*, 83rd ed.; CRC Press: New York, 2003.

(55) De Renzi, V.; Di Felice, R.; Marchetto, D.; R. Biagi. R.; del Pennino, U.; Selloni, A. *J. Phys. Chem. B* **2004**, *108*, 16−20.

(56) Anderson, S. E.; Nyberg, G. L. *J. Electron. Spectrosc. Relat. Phenom.* **1990**, *52*, 735−746.

(57) Hammer B.; Norskov, J. K. In *Chemisorption and Reactivity of Supported Clusters and Thin Films*; Lambert, R. M., Pacchioni, G.; Kluwer Academic: Dordrecht, The Netherlands, 1997; pp 285−351.

(58) Di Felice, R.; Selloni, A. *J. Chem. Phys.* **2004**, *120*, 4906−4914.

(59) Mariani, C.; Allegretti, F.; Corradini, V.; Contini, G.; Castro, V. D.; Baldacchini, C.; Betti, M. G. *Phys. Rev. B* **2002**, *66*, 115407. Ferretti A.; Di Felice, R. *Phys. Rev. B* **2004**, *70*, 115412.

(60) Tachibana, M.; Yoshizawa, K.; Ogawa, A.; Fujimoto, H.; Hoffmann, R. *J. Phys. Chem. B* **2002**, *106*, 12727−12736.

(61) Crespo, P.; Litran, R.; Rojas, T. C.; Multigner, M.; de la Fuente, J. M.; Sanchez-Lopez, J. C.; Garcia, M. A.; Hernando, A.; Penades, S.; Fernandez, A. *Phys. Rev. Lett.* **2004**, *93*, 087204.

(62) Fischer, D.; Curioni, A.; Andreoni, W. *Langmuir* **2003**, *19*, 3567−3571.

(63) Kondoh, H.; Iwasaki, M.; Shimada, T.; Amemiya, K.; Yokoyama, T.; Ohta, T.; Shimomura, M.; Kono, S. *Phys. Rev. Lett.* **2003**, *90*, 066102. Roper, M. G.; Skegg, M. P.; Fisher, C. J.; Lee, J. J.; Dhanak, V. R.; Woodruff, D. P.; Jones, R. G. *Chem. Phys. Lett.* **2004**, *389*, 87−91. Casalis L.; Cossaro, A.; Morgante, A.; Verdini, A.; Scoles, G. Unpublished data.